Journal of *Marine Science and Engineering*

MDPI

Article

A Prediction Method and Model Experiments on Surf-Riding and Broaching in Stern-Quartering Waves

Jilong Chu *, Min Gu, Jiang Lu and Peijie Zhang

China Ship Scientific Research Center, Wuxi 214082, China; gumin702@163.com (M.G.); lujiang1980@aliyun.com (J.L.); pjzhang@cssrc.com.cn (P.Z.)
* Correspondence: long8616767@163.com

Abstract: At present, the International Maritime Organization (IMO) has issued interim guidelines for the direct stability assessment of surf-riding and broaching for the second-generation intact stability criteria. Accurately and efficiently predicting surf-riding and broaching remains a key problem to be solved for the direct stability assessment of surf-riding and broaching. Therefore, a six-degree-of-freedom(6DOF) coupled mathematical model is established in this paper. Firstly, the four-degree-of-freedom(4DOF) coupled equations of surge–sway–roll–yaw motions are built based on the traditional MMG maneuvering mathematical model by considering Froude–Krylov forces, diffraction forces and restoring forces, and the heave and pitch are approximately calculated by iteratively solving improved static equilibrium equations in real-time, effectively solving the divergence problem in direct time-domain seakeeping calculations of high-speed ships in stern-quartering waves. Secondly, the hydrodynamic lift forces due to the coexistence of wave particle velocity and ship forward velocity are taken into account in the propeller-thrust and rudder-force models. In addition, the real-time emersion of twin rudders in waves is considered in the rudder-force models. At the same time, the free-running model experiments with a ONR tumblehome vessel are carried out in stern-quartering waves, and the pure loss of stability and broaching motions are observed. Finally, comparative validations between the calculations and the experiments of surf-riding and broaching in stern-quartering waves are carried out, and the effects of the ship speed, the instantaneous wetted surface of the hull, rudder exposure, heave and pitch motions on predicting surf-riding and broaching motions are investigated. The computation results show that the established 6DOF mathematical model has enough accuracy to be used for the direct stability assessment of the surf-riding and broaching failure modes.

Keywords: direct stability assessment; surf-riding; broaching; capsizing

Citation: Chu, J.; Gu, M.; Lu, J.; Zhang, P. A Prediction Method and Model Experiments on Surf-Riding and Broaching in Stern-Quartering Waves. *J. Mar. Sci. Eng.* **2024**, *12*, 1538. https://doi.org/10.3390/jmse12091538

Academic Editor: Decheng Wan

Received: 16 July 2024
Revised: 11 August 2024
Accepted: 14 August 2024
Published: 4 September 2024

1. Introduction

At present, the International Maritime Organization (IMO) has issued interim guidelines and corresponding explanatory notes on the second-generation intact stability criteria, covering three-tier stability assessment methods and operational guidance for the five stability failure modes of parametric rolling, pure loss of stability, dead ship condition, excessive acceleration and surf-riding/broaching [1,2]. Among the five stability failure modes, surf-riding/broaching is the most complex failure mode, which has a strong nonlinear characteristic and belongs to maneuverability problems in extreme seas. The prediction of surf-riding and broaching involves the cross-coupling of multiple disciplines, such as ship maneuverability, seakeeping, stability, resistance and propulsion. How to accurately and efficiently predict the surf-riding and broaching is a key issue that urgently needs to be solved in the direct stability assessment methods for surf-riding and broaching.

For the prediction of surf-riding and broaching, Umeda et al. [3] adopted a 4DOF maneuverability model, considering linear wave forces to qualitatively predict the surf-riding and broaching phenomenon of the ITTC A2 fishing vessels in regular waves. In order to

achieve the quantitative prediction of surf-riding and broaching, they successively analyzed the effects of nine nonlinear factors, including initial conditions, nonlinear maneuvering coefficients in still water, wave effects on linear maneuvering coefficients, wave effects on the roll-restoring arm, wave effects on rudder forces, nonlinear incident wave forces, wave effects on thrust, nonlinear coupling of sway and yaw and hydrodynamic forces due to large heel in still water and waves [4,5]. They established an "enhanced model" considering nine nonlinear factors, and the calculation results were in good agreement with the experimental results [6].

Subsequently, they applied this 4DOF mathematical model to predict the surf-riding and broaching phenomenon of the unconventional tumblehome ship with twin propellers and twin rudders, which can better predict the periodic motion region and surf-riding region. However, there is an obvious difference between the prediction results and experimental results for the broaching region [7]. In order to express the emergence of rudders and propellers to improve the prediction results for the broaching region, Araki et al. [8,9] established a 6DOF mathematical model by taking into account the effects of heave and pitch. Umeda et al. [10] used the 4DOF mathematical model to predict the broaching motion of the ONR flared ship in regular waves, and combined with the critical wave method to predict the probability of broaching in irregular waves. To improve the prediction results of the broaching region for the ONR tumblehome vessel using the 4DOF mathematical model, Htet et al. [11] modified the theoretical calculation formula based on the experiment measurement results of wave forces.

Spyrou et al. [12,13] discussed the definition the surf-riding in irregular waves based on the surge equation and assessed the probability of surf-riding based on two schemes. Belenky et al. [14] defined a critical distance in the phase plane of surge motion as a standard for judging the occurrence of surf-riding in irregular waves. Themelis et al. [15] adopted a 4DOF model to simulate the broaching and capsizing in irregular waves, and used a direct counting method to conduct statistical analysis for high-run, broaching and capsizing. Yu et al. [16] also adopted the direct counting method to calculate the probability of surf-riding and broaching based on a 6DOF model.

The accuracy of numerical prediction of surf-riding and broaching is crucial to evaluate the probability of surf-riding and broaching in irregular waves. Currently, there are few mathematical models that can accurately predict surf-riding and broaching. To provide an accurate and efficient prediction method of the surf-riding and broaching for the direct stability assessment, the first author and co-workers previously constructed a 4DOF mathematical model of surge–sway–roll–yaw motions considering nonlinear factors such as the emersion of rudders and propellers in waves, the diffraction effect of surge wave force, and nonlinear hydrodynamic derivatives, which can accurately predict the surf-riding of the ONR tumblehome vessel, except broaching [17]. In order to predict the broaching of this unconventional ship, a 6DOF coupled mathematical model is established based on the 4DOF MMG equations and improved static equilibrium equations.

2. Mathematical Model

2.1. Coordinate Systems

The following three coordinate systems are used, as shown in Figure 1. A space coordinate system $O-\xi,\eta,\zeta$, with the origin O located in the horizontal plane, and the ζ-axis oriented downward as positive, is defined. This coordinate system is used to describe waves, which propagate along the positive direction of the ξ-axis, and the wave trough is located at the origin O at the initial moment. A body system $G-x,y,z$ takes the center of gravity G of the ship as the origin, with the x-axis in the centerline plane of the ship, parallel to the base plane, pointing to the bow as positive, and the z-axis downward as positive. This coordinate system swings with the ship. A reference coordinate system $G-x',y',z'$ has the same origin with the body system [3]. This coordinate system follows the ship during surge, sway, heave and yaw movements, but does not follow the ship during roll and pitch.

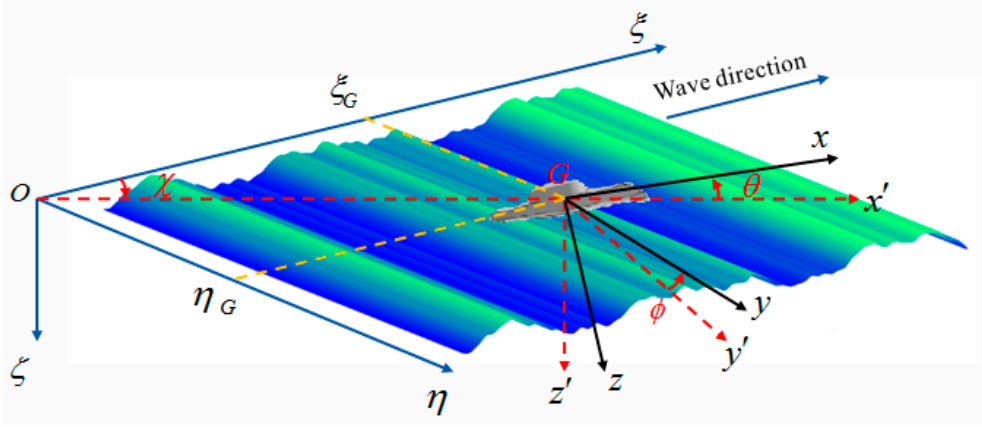

Figure 1. Coordinate systems.

As shown in Figure 1, ϕ, θ, δ is the roll angle, pitch angle and rudder angle, respectively. χ_C is desired heading angle of the ship, and χ is the instantaneous heading angle of the ship. ξ_G and η_G are, respectively, the longitudinal position and lateral position of the center of gravity G of the ship in the space coordinate system $O-\xi,\eta,\zeta$.

The conversion relations among the space coordinate system, the body coordinate system and the reference coordinate system are shown in Equations (1) and (2), respectively.

$$\begin{bmatrix} x' \\ y' \\ z' \end{bmatrix} = \begin{bmatrix} \cos\theta & \sin\phi\sin\theta & \cos\phi\sin\theta \\ 0 & \cos\phi & -\sin\phi \\ -\sin\theta & \sin\phi\cos\theta & \cos\phi\cos\theta \end{bmatrix} \begin{bmatrix} x \\ y \\ z \end{bmatrix} \tag{1}$$

$$\begin{bmatrix} \xi-\xi_G \\ \eta-\eta_G \\ \zeta-\zeta_G \end{bmatrix} = \begin{bmatrix} \cos\theta\ \cos\chi & \sin\phi\ \sin\theta\ \cos\chi & \cos\phi\ \sin\theta\ \cos\chi \\ & -\cos\phi\ \sin\chi & +\sin\phi\ \sin\chi \\ \cos\theta\ \sin\chi & \sin\phi\ \sin\theta\ \sin\chi & \cos\phi\ \sin\theta\ \sin\chi \\ & +\cos\phi\ \cos\chi & -\sin\phi\ \cos\chi \\ -\sin\theta & \sin\phi\ \cos\theta & \cos\phi\ \cos\theta \end{bmatrix} \begin{bmatrix} x \\ y \\ z \end{bmatrix} \tag{2}$$

2.2. 6DOF Motion Equations

The dynamic stability failure model of surf-riding and broaching in waves is a strong nonlinear phenomena. Broaching due to surf-riding in following and stern-quartering waves, which is frequently associated with the nonlinear large roll and yaw motions, is correlated with seakeeping, maneuvering, stability, resistance and propulsion. Currently, there are few mathematical models that can accurately predict surf-riding and broaching, so a 6DOF mathematical model based on modified 4DOF MMG equations and modified static equilibrium equations for predicting surf-riding and broaching is presented as follows.

The 4DOF coupled equations of surge–sway–roll–yaw motions are improved by adding wave diffraction forces, Froude–Krylov forces and restoring forces to the MMG standard model, as shown in Equations (3)–(6).

$$(m+m_x)\dot{u} - (m+m_y)vr = X_H + X_R + X_P + \mu X_{W\_FK} \tag{3}$$

$$(m+m_y)\dot{v} + (m+m_x)ur = Y_H + Y_R + Y_{W\_FK} + Y_{W\_Diff} \tag{4}$$

$$(I_{xx}+J_{xx})\dot{p} - m_x z_H ur = K_H + K_R + K_{W\_FK} + K_{W\_Diff} + K_{W\_Res} + (Y_{W\_FK} + Y_{W\_Diff})\overrightarrow{OG} \tag{5}$$

$$(I_{zz}+J_{zz})\dot{r} = N_H + N_R + N_P + N_{W\_FK} + N_{W\_Diff} \tag{6}$$

The subscripts H, R, P, W_FK, W_Diff and W_Res represent the hull force, the rudder force, the propeller thrust, the Froude–Krylov force, the diffraction force and the restoring force, respectively.

When a ship sails in following or stern-quartering waves at a high speed and the ratio of wavelength to length ratio is about one or larger, the ship encounter frequency may be very low or even zero. However, the calculations of radiation forces in heave and pitch directions at a low encounter frequency are easy to diverge, which may lead to heave and pitch motions divergence in the time-domain calculation.

Therefore, in order to obtain the steady heave and pitch of a ship sailing at high speed in following and stern-quartering waves, the improved static equilibrium equations are used to approximately calculate the instantaneous heave and pitch, as shown in Equations (7) and (8).

$$mg + Z_{\mathrm{W\_FK}} + Z_{\mathrm{W\_Res}} = 0 \tag{7}$$

$$M_{\mathrm{W\_FK}} + M_{\mathrm{W\_Res}} = 0 \tag{8}$$

In the above static equilibrium equations, it is assumed that the instantaneous equilibrium conditions are met: gravity, the instantaneous Froude–Krylov force and the restoring force are balanced in the heave direction, while the instantaneous Froude–Krylov moment and restoring moment are balanced in the pitch direction. The wave radiation forces and diffraction forces are ignored in these two directions, which can effectively solve the divergence problem in direct time-domain seakeeping calculations for the heave and pitch motions of high speed ships at a low encounter frequencies.

Roll, heave and pitch motions are coupled with each other in this 6DOF mathematical model because the Froude–Krylov forces and restoring forces in these three directions are calculated by integrating the pressure around the instantaneous wetted surface of the hull according to the simultaneous relative position of the ship to waves, which is related to the 6DOF instantaneous attitude of the ship and the instantaneous wave surface.

The PD control is adopted by the automatic control system of rudders to keep course, as shown in Equation (9).

$$\dot{\delta} = \{-\delta - K_{\mathrm{P}}(\chi - \chi_{\mathrm{C}}) - K_{\mathrm{P}}T_{\mathrm{D}}r\}/T_{\mathrm{E}} \tag{9}$$

The longitudinal position η_{G} and lateral position ξ_{G} of the ship in the space-fixed coordinate system $O-\xi,\eta,\zeta$ are obtained by the following equation.

$$\xi_{\mathrm{G}} = \int_0^t (u\cos\chi - v\sin\chi)dt \tag{10}$$

$$\eta_{\mathrm{G}} = \int_0^t (u\sin\chi + v\cos\chi)dt \tag{11}$$

2.3. Hull Forces in Still Water

The hull forces in still water $X_{\mathrm{H}}, Y_{\mathrm{H}}, N_{\mathrm{H}}$ and K_{H} are expressed as follows:

$$X_{\mathrm{H}} = -R(u) + X_{vv}v^2 + X_{vr}vr + X_{rr}r^2 \tag{12}$$

$$Y_{\mathrm{H}} = Y_v v + Y_r r + Y_{vvv}v^3 + Y_{vvr}v^2 r + Y_{vrr}vr^2 + Y_{rrr}r^3 \tag{13}$$

$$N_{\mathrm{H}} = N_v v + N_r r + N_{vvv}v^3 + N_{vvr}v^2 r + N_{vrr}vr^2 + N_{rrr}r^3 \tag{14}$$

$$K_{\mathrm{H}} = -D(p) - Y_{\mathrm{H}}z_{\mathrm{H}} \tag{15}$$

where $R\,(u)$ is the ship resistance in still water, which is expressed as follows:

$$R(u) = \frac{1}{2}\rho S_{\mathrm{F}}u^2 C_{\mathrm{T}}\left(\frac{u}{\sqrt{gL_{\mathrm{PP}}}}\right) \tag{16}$$

where C_{T} is total resistance coefficient, which is obtained by the resistance model experiment in still water.

$D(p)$ is the roll damping moment, which is expressed as follows:

$$D(p) = (I_{xx} + J_{xx})(\alpha \cdot p + \gamma \cdot p^3) \tag{17}$$

where α, γ are, respectively, the linear coefficient and the cubic coefficient of roll damping, which are obtained from the decay test of roll motion.

2.4. Propeller Thrust

In the temporary guidelines for direct stability failure assessment, there is a requirement for the surf-riding and broaching, which is that hydrodynamic forces caused by vortex shedding from a ship should be appropriately modeled. This should contain hydrodynamic lift forces induced by the coexistence of ship speed and wave particle velocity [1]. Therefore, the variation of the inflow velocity induced by wave particle velocity around propellers is considered.

The thrust X_P of twin propellers is expressed as follows (S: starboard; P: port):

$$X_P = T_P + T_S = (1 - t_P)\rho {n_P}^2 D_P^4 [K_T(J_{PP}) + K_T(J_{PS})] \tag{18}$$

$$N_P = -(T_P y_{PP} + T_S y_{PS}) = -(1 - t_P)\rho {n_P}^2 D_P^4 [K_T(J_{PP}) y_{PP} + K_T(J_{PS}) y_{PS}] \tag{19}$$

$$J_{PP} = \frac{(1 - w_P)(u - y_{PP} r) - u_{WPP}}{n_P D_P} \tag{20}$$

$$J_{PS} = \frac{(1 - w_P)(u - y_{PS} r) - u_{WPS}}{n_P D_P} \tag{21}$$

$$u_{WPP} = -\zeta_w \omega \cos\chi \exp(-k z_{PP}) \cos[k(\xi_G + x_{PP}\cos\chi - y_{PP}\sin\chi)] \tag{22}$$

$$u_{WPS} = -\zeta_w \omega \cos\chi \exp(-k z_{PS}) \cos[k(\xi_G + x_{PS}\cos\chi - y_{PS}\sin\chi)] \tag{23}$$

2.5. Rudder Forces

Similar to the propeller thrust, the variation of the inflow velocity induced by wave particle velocity around rudders is considered.

Furthermore, broaching is always accompanied by a large roll, and the significantly large roll will result in the frequent emersion of the twin rudders in waves. Therefore, the 6DOF mathematical model is modified to take account of the variation of the rudder force by considering rudders emersion in waves (Figure 2).

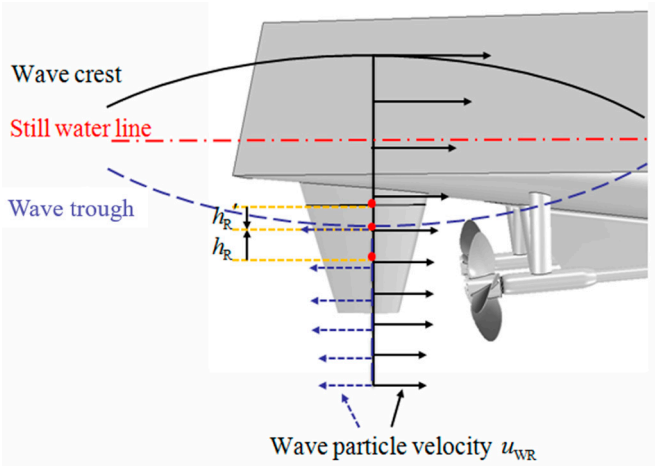

Figure 2. Wave particle velocity around rudders and propellers.

The rudder forces of X_R, Y_R, N_R and K_R with rudder emersion and wave particle velocity are rewritten in the Formulas (24)–(40), as referenced in [18] (S: starboard; P: port):

$$X_R = X_{RP} + X_{RS} = -(1 - t_R)F_{NP}\sin\delta - (1 - t_R)F_{NS}\sin\delta \tag{24}$$

$$Y_{\mathrm{R}} = -(1 + a_{\mathrm{H}})(F_{\mathrm{NP}} + F_{\mathrm{NS}})\cos\delta \tag{25}$$

$$N_{\mathrm{R}} = -(x_{\mathrm{R}} + a_{\mathrm{H}}x_{\mathrm{HR}})(F_{\mathrm{NP}} + F_{\mathrm{NS}})\cos\delta - (y_{\mathrm{RP}}X_{\mathrm{RP}} + y_{\mathrm{RS}}X_{\mathrm{RS}}) \tag{26}$$

$$K_{\mathrm{R}} = (z_{\mathrm{R}} + a_{\mathrm{H}}z_{\mathrm{HR}})(F_{\mathrm{NP}} + F_{\mathrm{NS}})\cos\delta \tag{27}$$

where

$$F_{\mathrm{NP}} = \frac{1}{2}\rho A_{\mathrm{RP}}U_{\mathrm{RP}}^2 f_{\alpha\mathrm{P}}\sin\alpha_{\mathrm{RP}},\ F_{\mathrm{NS}} = \frac{1}{2}\rho A_{\mathrm{RS}}U_{\mathrm{RS}}^2 f_{\alpha\mathrm{S}}\sin\alpha_{\mathrm{RS}} \tag{28}$$

$$U_{\mathrm{RP}} = \sqrt{u_{\mathrm{RP}}^2 + v_{\mathrm{R}}^2},\ U_{\mathrm{RS}} = \sqrt{u_{\mathrm{RS}}^2 + v_{\mathrm{R}}^2} \tag{29}$$

$$f_{\alpha\mathrm{P}} = \frac{6.13\Lambda_{\mathrm{P}}}{2.25 + \Lambda_{\mathrm{P}}},\ f_{\alpha\mathrm{S}} = \frac{6.13\Lambda_{\mathrm{S}}}{2.25 + \Lambda_{\mathrm{S}}} \tag{30}$$

$$\alpha_{\mathrm{RP}} = \delta - \frac{v_{\mathrm{R}}}{u_{\mathrm{RP}}},\ \alpha_{\mathrm{RS}} = \delta - \frac{v_{\mathrm{R}}}{u_{\mathrm{RS}}} \tag{31}$$

$$v_{\mathrm{R}} = \overline{\gamma_{\mathrm{R}}}U(\beta - \overline{\overset{\curvearrowleft}{\downarrow}_{\mathrm{R}}r'}) \tag{32}$$

$$u_{\mathrm{RP}} = \varepsilon(1 - w_{\mathrm{p}})u\sqrt{\eta\left\{1 + \kappa\left(\sqrt{1 + \frac{8K_{\mathrm{T}}(J_{\mathrm{PP}})}{\pi J_{\mathrm{PP}}^2}} - 1\right)\right\}^2 + 1 - \eta} - u_{\mathrm{WRP}} \tag{33}$$

$$u_{\mathrm{RS}} = \varepsilon(1 - w_{\mathrm{p}})u\sqrt{\eta\left\{1 + \kappa\left(\sqrt{1 + \frac{8K_{\mathrm{T}}(J_{\mathrm{PS}})}{\pi J_{\mathrm{PS}}^2}} - 1\right)\right\}^2 + 1 - \eta} - u_{\mathrm{WRS}} \tag{34}$$

$$u_{\mathrm{WRP}} = -\zeta_{\mathrm{w}}\omega\cos\chi\exp(-kz_{\mathrm{RP}})\cos[k(\xi_{\mathrm{G}} + x_{\mathrm{RP}}\cos\chi - y_{\mathrm{RP}}\sin\chi)] \tag{35}$$

$$u_{\mathrm{WRS}} = -\zeta_{\mathrm{w}}\omega\cos\chi\exp(-kz_{\mathrm{RS}})\cos[k(\xi_{\mathrm{G}} + x_{\mathrm{RS}}\cos\chi - y_{\mathrm{RS}}\sin\chi)] \tag{36}$$

$$A_{\mathrm{RP}} = A_{\mathrm{R}} + (h_{\mathrm{RP}} - 0.5\sqrt{A_{\mathrm{R}}\Lambda})\sqrt{\frac{A_{\mathrm{R}}}{\Lambda}}\ (if\ (h_{\mathrm{RP}} - 0.5\sqrt{A_{\mathrm{R}}\Lambda}) < 0)) \tag{37}$$

$$A_{\mathrm{RS}} = A_{\mathrm{R}} + (h_{\mathrm{RS}} - 0.5\sqrt{A_{\mathrm{R}}\Lambda})\sqrt{\frac{A_{\mathrm{R}}}{\Lambda}}\ (if\ (h_{\mathrm{RS}} - 0.5\sqrt{A_{\mathrm{R}}\Lambda}) < 0)) \tag{38}$$

$$\Lambda_{\mathrm{p}} = [\sqrt{A_{\mathrm{R}}\Lambda} + (h_{\mathrm{RP}} - 0.5\sqrt{A_{\mathrm{R}}\Lambda})]/\sqrt{A_{\mathrm{R}}/\Lambda} \tag{39}$$

$$\Lambda_{\mathrm{S}} = [\sqrt{A_{\mathrm{R}}\Lambda} + (h_{\mathrm{RS}} - 0.5\sqrt{A_{\mathrm{R}}\Lambda})]/\sqrt{A_{\mathrm{R}}/\Lambda} \tag{40}$$

2.6. Wave Forces

The wave forces, including wave diffraction forces, Froude–Krylov forces and restoring forces, are rewritten in the Formulas (41)–(49), as referenced in [7].

$$X_{\mathrm{W\_FK}} = -\mu_x\rho g\zeta_{\mathrm{w}}k\cos\chi\int_{AE}^{FE} C_1(x)S(x)e^{-kd(x)/2}\sin k(\xi_{\mathrm{G}} + x\cos\chi)dx \tag{41}$$

$$Y_{\mathrm{W\_FK}} = \rho g\zeta_{\mathrm{w}}k\sin\chi\int_{AE}^{FE} C_1(x)S(x)e^{-kd(x)/2}\sin k(\xi_{\mathrm{G}} + x\cos\chi)dx \tag{42}$$

$$\begin{aligned} Y_{\mathrm{W\_Diff}} &= \zeta_{\mathrm{w}}\omega\omega_{\mathrm{e}}\sin\chi\textstyle\int_{AE}^{FE}\rho S_y(x)e^{-kd(x)/2}\sin k(\xi_{\mathrm{G}} + x\cos\chi)dx \\ &-\zeta_{\mathrm{w}}\omega u\sin\chi\left[\rho S_y(x)e^{-kd(x)/2}\cos k(\xi_{\mathrm{G}} + x\cos\chi)\right]_{AE}^{FE} \end{aligned} \tag{43}$$

$$N_{\mathrm{W\_FK}} = \rho g\zeta_{\mathrm{w}}k\sin\chi\int_{AE}^{FE} C_1(x)S(x)e^{-kd(x)/2}x\sin k(\xi_{\mathrm{G}} + x\cos\chi)dx \tag{44}$$

$$\begin{aligned} N_{\mathrm{W\_Diff}} &= \zeta_{\mathrm{w}}\omega\omega_{\mathrm{e}}\sin\chi\textstyle\int_{AE}^{FE}\rho S_y(x)e^{-kd(x)/2}x\sin k(\xi_{\mathrm{G}} + x\cos\chi)dx \\ &+\zeta_{\mathrm{w}}\omega u\sin\chi\textstyle\int_{AE}^{FE}\rho S_y(x)e^{-kd(x)/2}\cos k(\xi_{\mathrm{G}} + x\cos\chi)dx \\ &-\zeta_{\mathrm{w}}\omega u\sin\chi\left[\rho S_y(x)e^{-kd(x)/2}x\cos k(\xi_{\mathrm{G}} + x\cos\chi)\right]_{AE}^{FE} \end{aligned} \tag{45}$$

$$K_{\mathrm{W\_Re}} = -mgGZ(\phi) \tag{46}$$

$$K_{\mathrm{W\_FK}} = \rho g \zeta_{\mathrm{w}} k \sin\chi \int_{AE}^{FE} C_4(x) \left\{ \frac{B(x)}{2} \right\}^3 e^{-kd(x)} \sin k(\xi_{\mathrm{G}} + x\cos\chi) dx$$
$$-\rho g \frac{\zeta_{\mathrm{w}}}{k} \sin\chi \int_{AE}^{FE} C_1(x) B(x) \left\{ 1 - (1 + kd(x)) e^{-kd(x)} \right\} \sin k(\xi_{\mathrm{G}} + x\cos\chi) dx \quad (47)$$

$$K_{\mathrm{W\_Diff}} = -\zeta_{\mathrm{w}} \omega \omega_{\mathrm{e}} \sin\chi \int_{AE}^{FE} \rho S_y l_\eta(x) e^{-kd(x)/2} \sin k(\xi_{\mathrm{G}} + x\cos\chi) dx$$
$$+\zeta_{\mathrm{w}} \omega u \sin\chi \left[\rho S_y l_\eta(x) e^{-kd(x)/2} \cos k(\xi_{\mathrm{G}} + x\cos\chi) \right]_{AE}^{FE} \quad (48)$$

$$\begin{aligned} \mu_x &= 1.46 C_{\mathrm{b}} - 0.05 \; for \; C_{\mathrm{m}} < 0.86 \\ &= (5.76 - 5.00 C_{\mathrm{m}}) C_{\mathrm{b}} - 0.05 \; for \; 0.86 < C_{\mathrm{m}} < 0.94 \\ &= 1.06 C_{\mathrm{b}} - 0.05 \; for \; C_{\mathrm{m}} \geq 0.94 \end{aligned} \quad (49)$$

where $S(x)$ is the submerged area of a ship section in still water, $B(x)$ is the waterline breadth of a ship section in still water, and $d(x)$ is the draft of a ship section in still water. μ_x is a correction coefficient for wave diffraction effect on surge motion, as shown in Equation (49) [19].

Broaching is frequently accompanied by a large roll, which is a problem related to the nonlinear variation of wave moments in the roll direction. Therefore, for the prediction of surf-riding and broaching, the nonlinear wave moment in roll direction is the key to improving the prediction accuracy for roll motion.

The nonlinear roll Froude–Krylov moments and the nonlinear roll-restoring moment in waves are calculated by integrating the pressure around the instantaneous wetted surface of the hull, which is determined according to the 6DOF instantaneous attitude of the ship and the instantaneous wave surface, as referenced in [20].

$$K_{\mathrm{W\_Re}} = -\rho g \int_{AE}^{FE} y(x) A(x) dx \quad (50)$$

$$K_{\mathrm{W\_FK}} = -\rho g \sin\chi \int_{AE}^{FE} z(x) F(x) A(x) \sin k(\xi_{\mathrm{G}} + x\cos\chi) dx \quad (51)$$

$$F(x) = \zeta_{\mathrm{w}} k \frac{\sin(k\frac{B(x)}{2}\sin\chi)}{k\frac{B(x)}{2}\sin\chi} e^{-kd(x)} \quad (52)$$

where $A(x)$ is the instantaneous submerged area of a ship section in waves, $y(x)$ is the instantaneous transverse position of a centroid of a ship section in the reference coordinate system $G - x', y', z'$, and $z(x)$ is the instantaneous vertical position of a centroid of a ship section in the reference coordinate system $G - x', y', z'$.

2.7. Heave and Pitch Motions

Using linear theory, the coupled static equilibrium equation of heave–pitch motions is transformed into the following equation:

$$mg + Z_{\mathrm{W\_FK}} + Z_{\mathrm{W\_Res}} = \rho \mathrm{g} \cdot \delta\zeta_{\mathrm{G}} \cdot \int_{AE}^{FE} B(x) dx \quad (53)$$

$$M_{\mathrm{W\_FK}} + M_{\mathrm{W\_Res}} = \rho \mathrm{g} \cdot \delta\theta \cdot \int_{AE}^{FE} x^2 B(x) dx \quad (54)$$

$$Z_{\mathrm{W\_Res}} = -\rho g \int_{AE}^{FE} A(x) dx \quad (55)$$

$$Z_{\mathrm{W\_FK}} = -\rho g \int_{AE}^{FE} F(x) A(x) \cos k(\xi_{\mathrm{G}} + x\cos\chi) dx \quad (56)$$

$$M_{\mathrm{W\_Res}} = \rho g \int_{AE}^{FE} x A(x) dx \quad (57)$$

$$M_{\mathrm{W\_FK}} = \rho g \int_{AE}^{FE} x F(x) A(x) \cos k(\xi_{\mathrm{G}} + x\cos\chi) dx \quad (58)$$

The variations in heave and pitch $(\delta\zeta_G, \delta\theta)$ are solved by using the bisection method, considering the mutual influence between $\delta\zeta_G$ and $\delta\theta$. When the conditions of $\delta\zeta_G \leq d/500$ and $\delta\theta \leq d/Lpp/500$ are met, the loop iteration is terminated, and finally heave and pitch are obtained.

Similar to the roll direction, the nonlinear Froude–Krylov force/moment and nonlinear restoring force/moment in the directions of heave and pitch are calculated by integrating the pressure around the instantaneous wetted hull surface.

3. Experiments

To validate the accuracy of the established 6DOF mathematical model for the numerical prediction of surf-riding and broaching, a free running model experiment with an ONR tumblehome vessel was carried out in stern-quartering waves.

The free-running model experiment was conducted in the large seakeeping and maneuvering basin of the China Ship Scientific Research Center. The basin is 170 m long, 47 m wide and 6 m deep and outfitted with flap wave makers on both vertical sides of the basin.

The ONR tumblehome vessel is a typical unconventional high-speed ship as a standard model for the second-generation intact stability criteria, which has good performance of propulsion and seakeeping due to some unique characteristics, such as a tumblehome superstructure, a wave-piercing bow, twin propellers and twin rudders.

The principal parameters of the ONR tumblehome vessel at full scale and model scale are shown in Table 1. The scale ratio of the actual ship to the model is 40.526. The whole model, bow and stern of the ship model are shown in Figure 3. Due to the risk of capsizing during the model experiment, the ship model must be made watertight. The ship model has bilge keels and no superstructure.

Table 1. The main parameters of the ONR tumblehome vessel.

Items	Full Scale	Model Scale
Length (L_{PP})	154.0 m	3.800 m
Draft (d)	5.494 m	0.136 m
Breadth (B)	18.8 m	0.464 m
Depth (D)	14.5 m	0.358 m
Displacement (W)	8507 ton	0.128 ton
Block coefficient C_B	0.535	0.535
Metacentric height GM	2.068 m	0.051 m
Vertical position of the center of gravity KG	7.672 m	0.189 m
Natural roll period T_{roll}	11.14 s	1.75 s
Roll inertia radius K_{xx}	0.44 B	0.44 B
Pitch inertia radius K_{yy}	0.25 L_{PP}	0.25 L_{PP}
Rudder area A_R	23.74 m^2	0.0145 m^2
Propeller diameter D_P	5.22 m	0.129 m

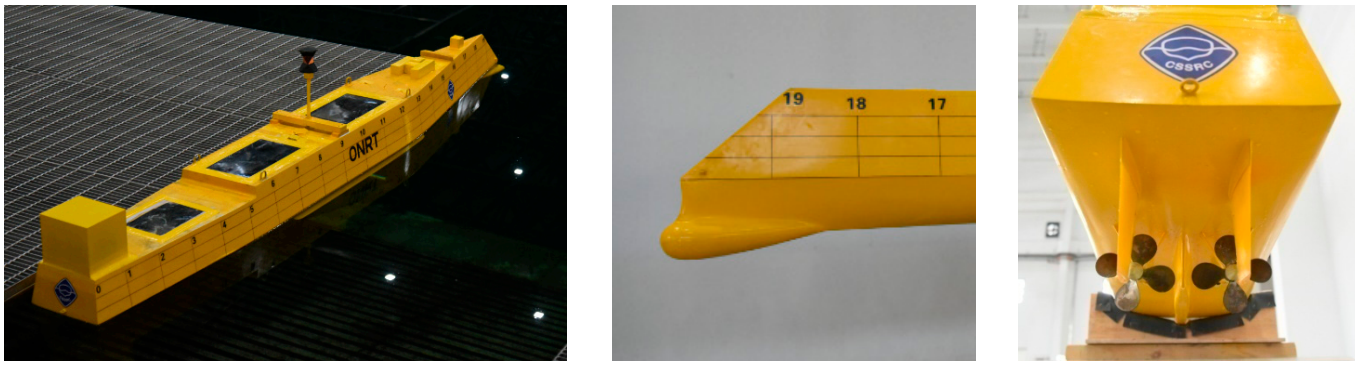

(**a**) whole model (**b**) bow (**c**) stern

Figure 3. The ship model of the ONR tumblehome vessel.

Unlike conventional maneuverability experiments, surf-riding and broaching experiments belong to stability experiments, and metacentric height is crucial to the broaching motion. Therefore, after adjusting the inertia of the ship model, it is necessary to adjust the weights positions according to the inclining test method to calibrate the initial metacentric height.

A free decay test of roll motion in still water was carried out to obtain the nonlinear damping coefficients. The revolution rates of the propellers corresponding to the nominal speeds of the ship in still water were obtained by measuring the real-time position of the ship model with the total station in the free-running experiment, and then the same revolution rates of the propellers in still water were used to achieve the same nominal speed of the ship in the free-running experiments in stern-quartering waves. A PD control system was applied to keep course by yaw velocity and the deflection between real-time heading angle and the desired heading angle.

The ship model was free running with the desired revolution rate of propellers along the long side of the basin. The waves were created by the wave makers on both-sides at a 30-degree angle to the long side, as shown in Figure 4. The yaw, roll and pitch were measured by a 6DOF optical fiber gyroscope based on MEMS (Micro Electro-Mechanical System) placed on the ship model. The real-time data of yaw, roll, pitch, rudder angle and revolution rate of the propellers were recorded by an on-board integrated device wirelessly. The wave elevation near the starting position of the ship model was measured by a servo-needle wave height sensor fixed to a steel bridge spanning over the basin. The real-time speed of the ship model was determined by the real-time position of the ship model in the free-running experiment, recorded by a total station.

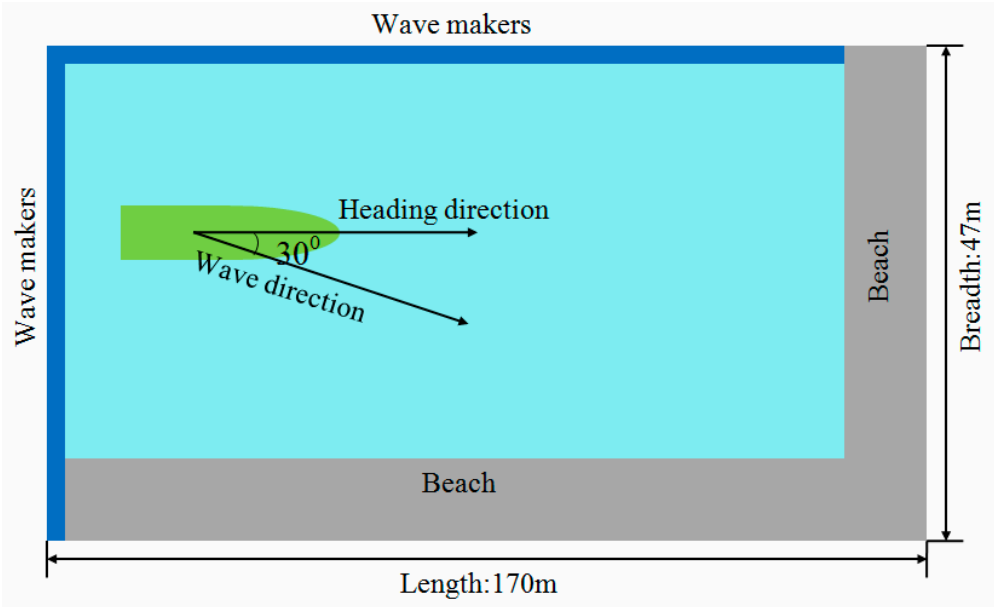

Figure 4. Wave direction and heading direction of the ship model.

Conditions and results of model experiments are shown in Table 2. The change process of typical pure loss of stability and broaching motions were observed in the model experiments, as shown in Figure 5. When the Froude number *Fn* of the ship model was equal to 0.3, the typical pure loss of stability occurred, and the maximum roll angle of the ship model reached about 30 degrees. However, when the *Fn* of the ship model was equal to 0.4, the typical broaching occurred, and the maximum roll angle and yaw angle of the ship model reached about 43.4 degrees and 26.9 degrees, respectively.

Table 2. Conditions and results of model experiments.

No.	Experiments Conditions			Experiments Results		
	λ/Lpp	H/λ	*Fn*	Maximum Roll Angle (Degree)	Maximum Yaw Angle (Degree)	Motion Modes
1	1.25	0.05	0.250	19.6	8.3	Pure loss of stability
2	1.25	0.05	0.300	28.0	11.3	Pure loss of stability
3	1.25	0.05	0.325	32.6	9.5	Pure loss of stability
4	1.25	0.05	0.350	35.3	13.2	Pure loss of stability
5	1.25	0.05	0.400	43.4	26.9	Broaching

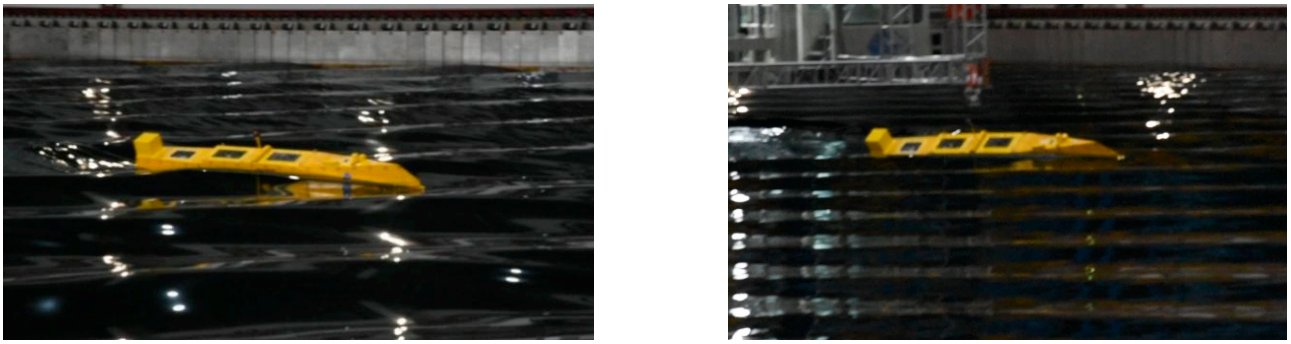

(**a**) pure loss of stability (*Fn* = 0.3) (**b**) broaching (*Fn* = 0.4)

Figure 5. The snapshots of pure loss of stability and broaching (λ/Lpp = 1.25, H/λ = 0.05, $\chi = -30°$).

4. Simulations and Discussions

4.1. The Effect of Ship Speed

To validate the proposed 6DOF mathematical model, the time-domain calculations are performed with the wave conditions of λ/Lpp = 1.25, H/λ = 0.05, $\chi = -30$ degrees. The comparison of time histories of roll, pitch, yaw and rudder angle for the different Froude numbers between the calculation results and the experimental results are shown in Figures 6–9, and the time-domain variation curves of the ratio of surge speed to wave speed for the different Froude numbers in the calculation results are shown in Figure 10. The initial conditions of the calculations are set according to the data measured in the experiments.

The trend of the calculation results and the experimental results with the different ship speeds is analyzed. At a low ship speed (*Fn* = 0.25), the calculation results are in good agreement with the experimental results. From the time history of the roll motion, it can be observed that the roll period of the ONR tumblehome vessel increases after three cycles. This is because when the ship approaches the wave crest, the ship speed increases under the action of wave force, and the relative speed between the ship and the wave decreases. Therefore, the time for the ship to pass through the wave crest increases, and the entire roll period also increases. This indicates that pure loss of stability occurs, and the mathematical model can predict this phenomenon well.

In addition, there is a significant deviation in roll motion, namely, the mean roll angle is larger than zero, and this phenomenon is also very well captured in the calculation results. There is also a noticeable deviation in yaw motion, but the yaw deviation in the calculation results is smaller than that in the experimental results. This phenomenon may be caused by the wave drift force, which is not considered in the mathematical model. This issue should be further investigated.

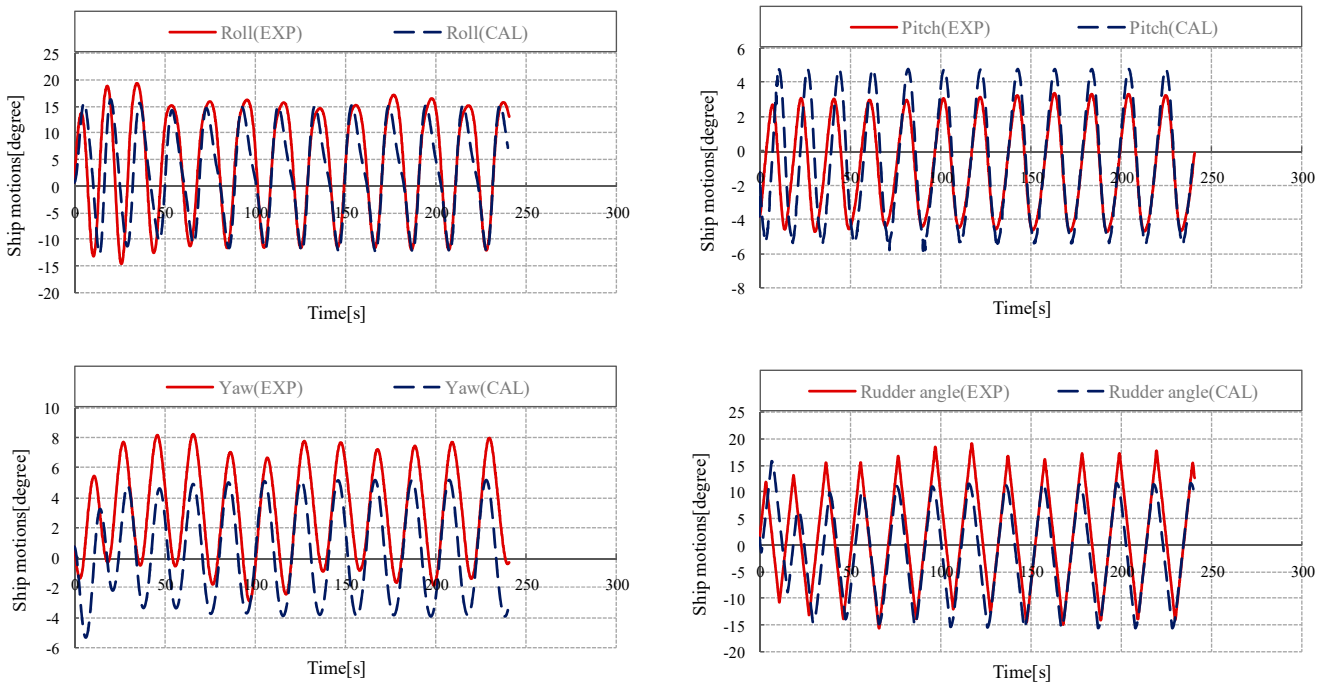

Figure 6. Comparison of time histories of ship motion with Fn = 0.25 (EXP: the experimental results; CAL: the calculation results).

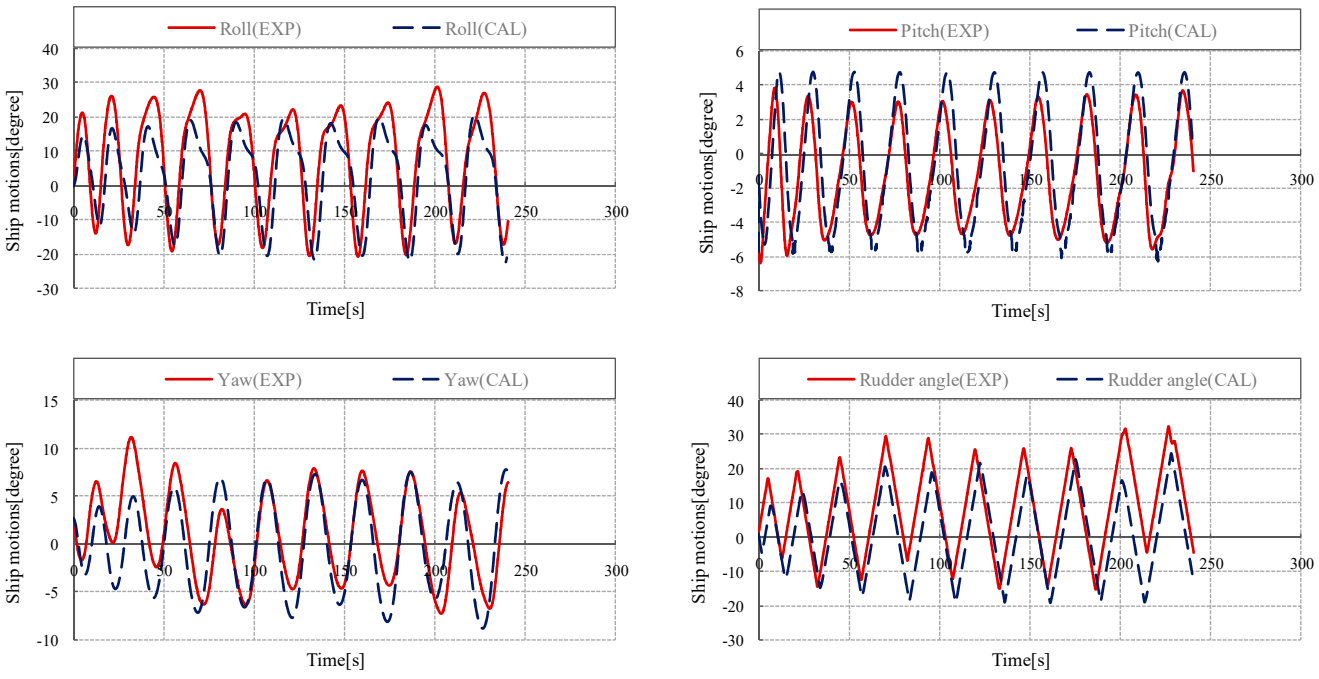

Figure 7. Comparison of time histories of ship motion with Fn = 0.30 (EXP: the experimental results; CAL: the calculation results).

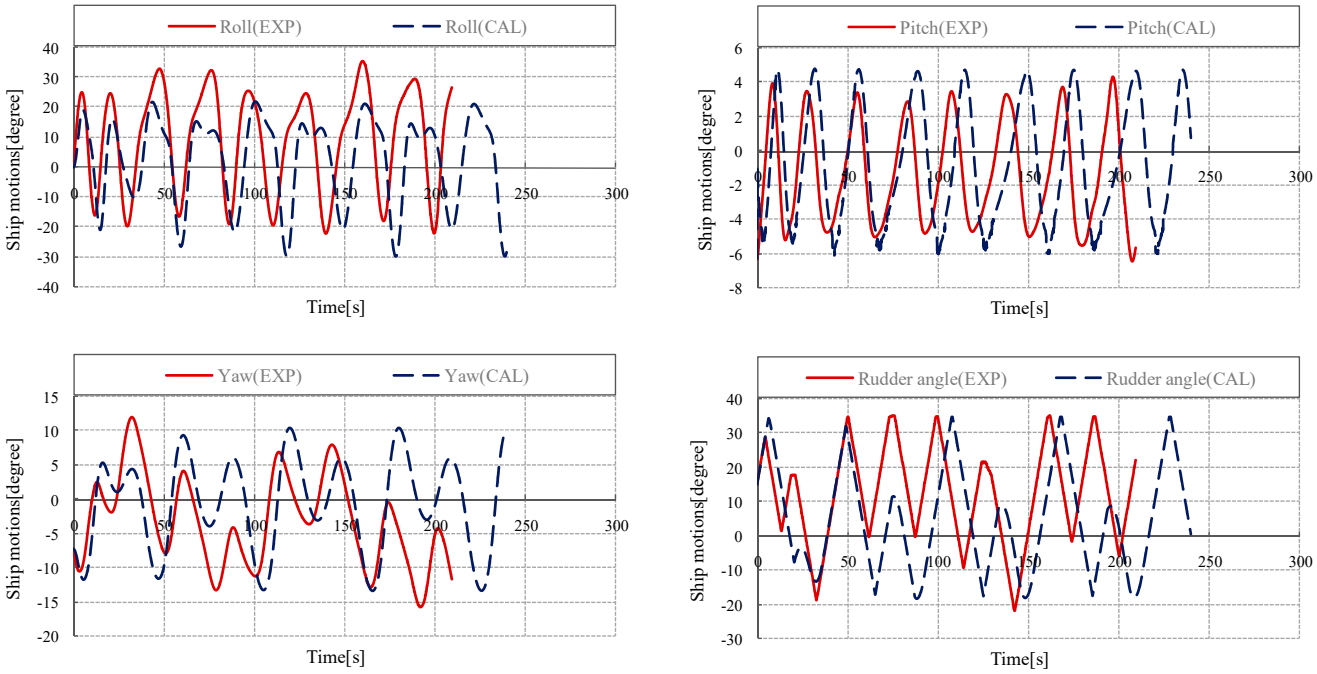

Figure 8. Comparison of time histories of ship motion with Fn = 0.35 (EXP: the experimental results; CAL: the calculation results).

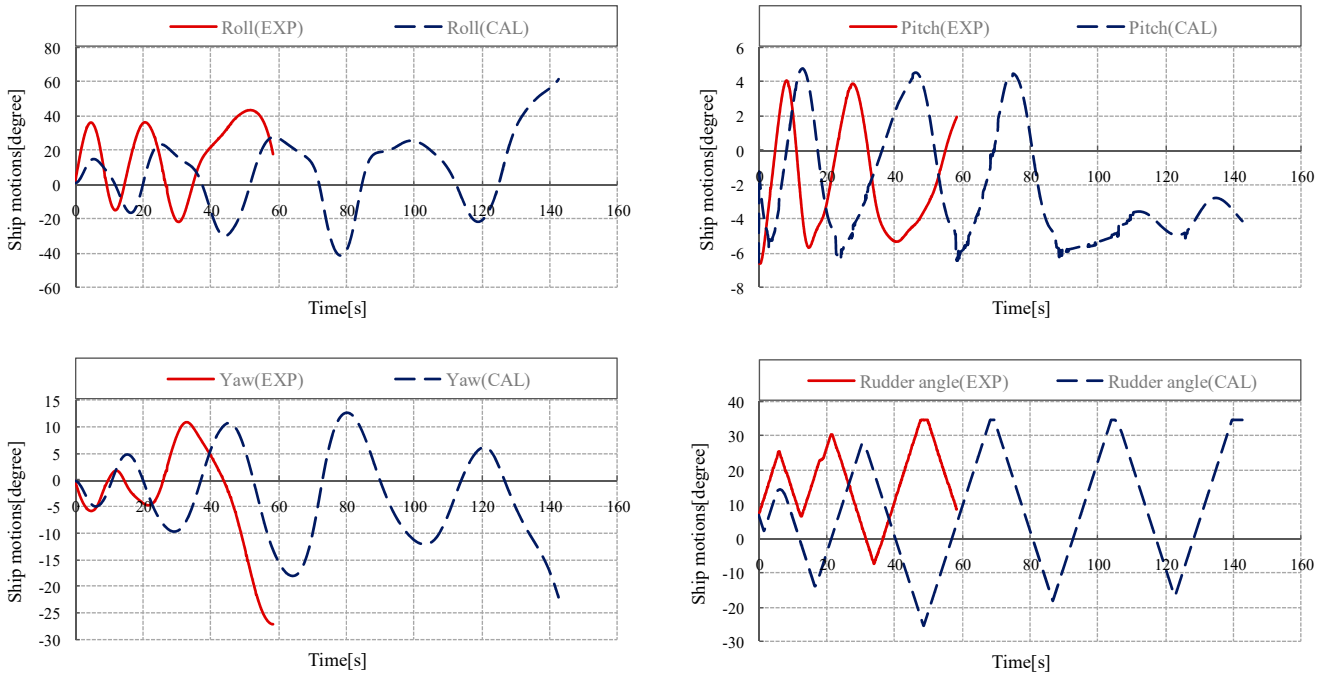

Figure 9. Comparison of time histories of ship motion with Fn = 0.40 (EXP: the experimental results; CAL: the calculation results).

As the ship speed increases (Fn = 0.3), the roll amplitude significantly increases, and the roll period also significantly increases after two roll periods. Under this condition, pure loss of stability occurs too. The calculation results are also in good agreement with the experimental results.

As the ship speed continues to increase (Fn = 0.35), the ONR tumblehome vessel still experiences pure loss of stability, but the time histories of yaw motion and rudder angle exhibit obvious irregular periodic variations, which are also captured in the calculation.

Because the ONR tumblehome vessel is in a critical state between pure loss of stability and surf-riding or broaching, the control of yaw motion becomes unstable.

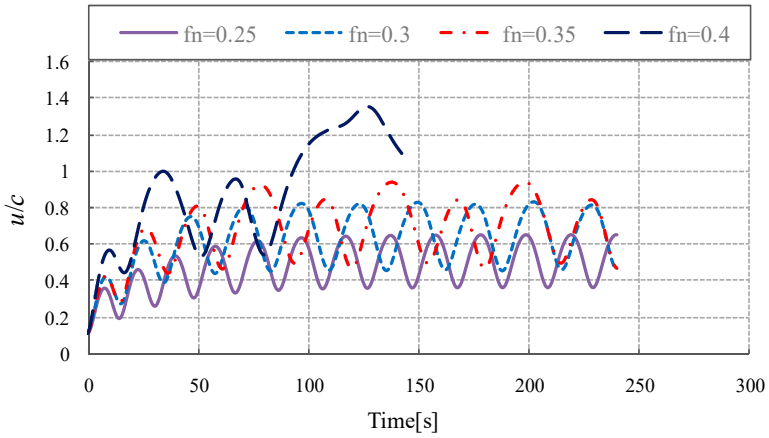

Figure 10. The ratio of ship speed to wave speed with different Froude numbers in calculation results.

When the ship speed reaches 30 knots (Fn = 0.4), the ONR tumblehome vessel experiences a large angle yaw in the calculation and the experiment. Even if the rudder angle is turned to the maximum value (+35 degrees), the heading remains unstable. This reveals that the ship experiences significant broaching motion. The maximum deflection of the heading angle is 26.8 degrees in the experiment, and the maximum deflection of the heading angle is 22 degrees in the calculation.

The maximum roll angle in the experiment reaches 43.4 degrees, while the roll angle in the calculation gradually increases up to 90 degrees until the ship capsizes. When the roll angle exceeds 60 degrees, the iterative solutions of the static balance equations cause large jump points in the heave and pitch motions, which are then truncated and deleted. However, it is difficult to right the ship when the roll angle is greater than 60 degrees, which does not affect the judgment of broaching and capsizing.

From the time histories of the surge speeds in Figure 10, it can be seen that the ratio of ship speed to wave speed is greater than 1 under this condition. The ONR tumblehome vessel experiences broaching caused by surf-riding, and the ship eventually capsizes in the calculation. However, the ship model experiences broaching but not capsizing in the experiment. When broaching occurs, the ship model turns left towards the wave maker, as shown in Figure 4. To ensure the safety of the wave maker due to the limitation of the basin width, the broaching motion of the ship model is ended in advance in the experiment. Therefore, it is not known whether the ship model will capsize in the experiment. To solve this problem, we can adjust the wave direction to make the ship model turn to the wave-absorbing shore on the other side of the basin in a future study.

From the above analysis, it can be seen that as the ship speed increases, the ship motion mode transitions from pure loss of stability to broaching.

4.2. The Effect of the Instantaneous Wetted Surface of the Hull

The effect of the instantaneous wetted surface of the hull on the ship motion mode is analyzed, and the comparison results of motion time histories with and without considering the instantaneous wetted surface of the hull are shown in Figures 11–13. GZlinear represents the roll Froude–Krylov moments and the roll-restoring moment in waves, calculated by integrating the pressure around the calm water surface, as described in Formulas (46) and (47). In addition, GZnonlinear represents the roll Froude–Krylov moments and roll-restoring moment in waves, calculated by integrating the pressure around the instantaneous wet surface of the hull, as described in Formulas (50) and (51).

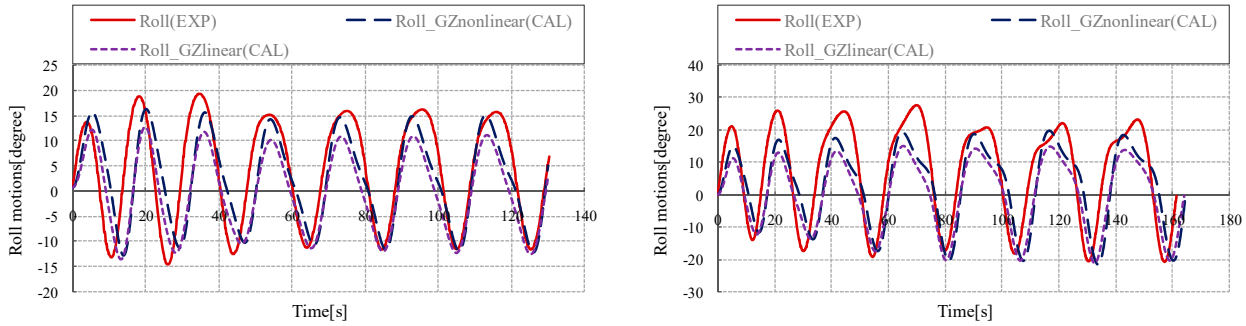

(**a**) Fn = 0.25 (**b**) Fn = 0.3

Figure 11. Comparison of time histories of roll motion with Fn = 0.25 and Fn = 0.3 (GZlinear (CAL): the calculation results without considering the instantaneous wetted surface of the hull; GZnonlinear (CAL): the calculation results considering the instantaneous wetted surface of the hull; EXP: the experimental results).

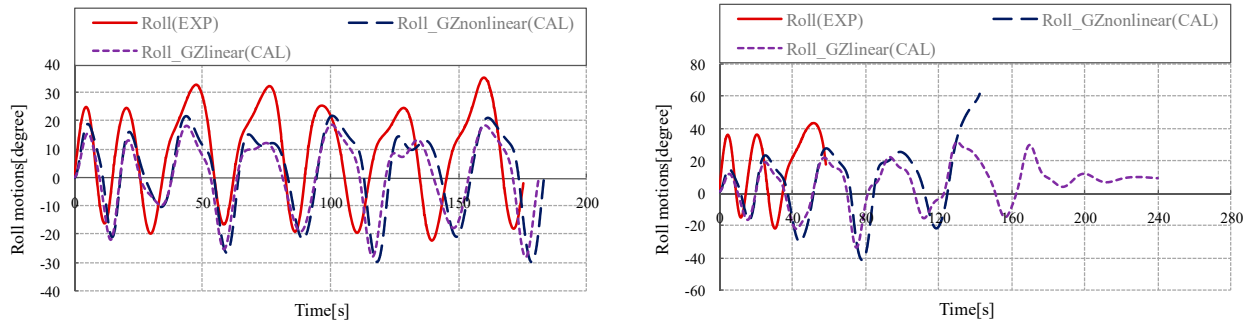

(**a**) Fn = 0.35 (**b**) Fn = 0.4

Figure 12. Comparison of time histories of roll motion with Fn = 0.35 and Fn = 0.4 (GZlinear (CAL): the calculation results without considering the instantaneous wetted surface of the hull; GZnonlinear (CAL): the calculation results considering the instantaneous wetted surface of the hull; EXP: the experimental results).

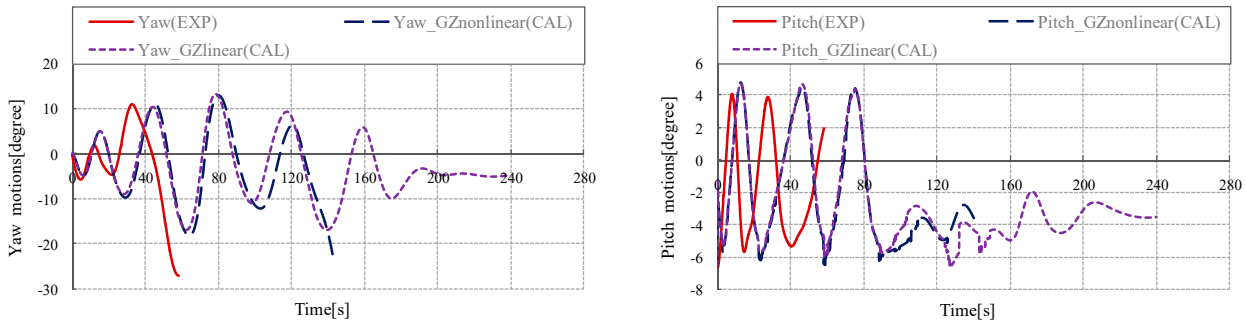

Figure 13. Comparison of time histories of yaw and pitch motions with Fn = 0.4 (GZlinear (CAL): the calculation results without considering the instantaneous wetted surface of the hull; GZnonlinear (CAL): the calculation results considering the instantaneous wetted surface of the hull; EXP: the experimental results).

Both methods can effectively simulate the periodic variations of roll motions, in which the time of the ship passing through the wave crest is greater than the time of the ship passing through the wave trough. At a low ship speed (Fn = 0.25), considering the nonlinearity of the instantaneous wetted surface of the hull, a steady heel is clearly simulated, and the calculated roll amplitude is closer to the experimental value. As the

ship speed increases (Fn = 0.30, 0.35), the nonlinear variation in roll motion becomes more pronounced. The roll amplitude calculated with instantaneous wetted surface is slightly larger than that calculated without instantaneous wetted surface, but both are smaller than the experimental values. At a high ship speed (Fn = 0.4), the amplitudes of roll, yaw and pitch motions calculated with the instantaneous wetted surface gradually increase until the ship capsizes. However, the amplitudes of roll, yaw and pitch motions calculated without the instantaneous wetted surface gradually stabilize to constant values, and the ship ultimately reaches a stable surf-riding state. This indicates that the nonlinearity of roll due to the instantaneous wetted surface of the hull has a significant effect on the prediction of broaching.

4.3. The Effect of Rudder Exposure

The effect of rudder exposure on ship motion modes is analyzed. The comparison results of time histories of ship motions with and without considering the rudder exposure in waves are shown in Figures 14 and 15, and the corresponding real-time submerged areas of twin rudders in waves are shown in the Figure 16. RudderOUT represents the calculations considering the rudder exposure in waves, and RudderIN represents the calculations without considering the rudder exposure in waves.

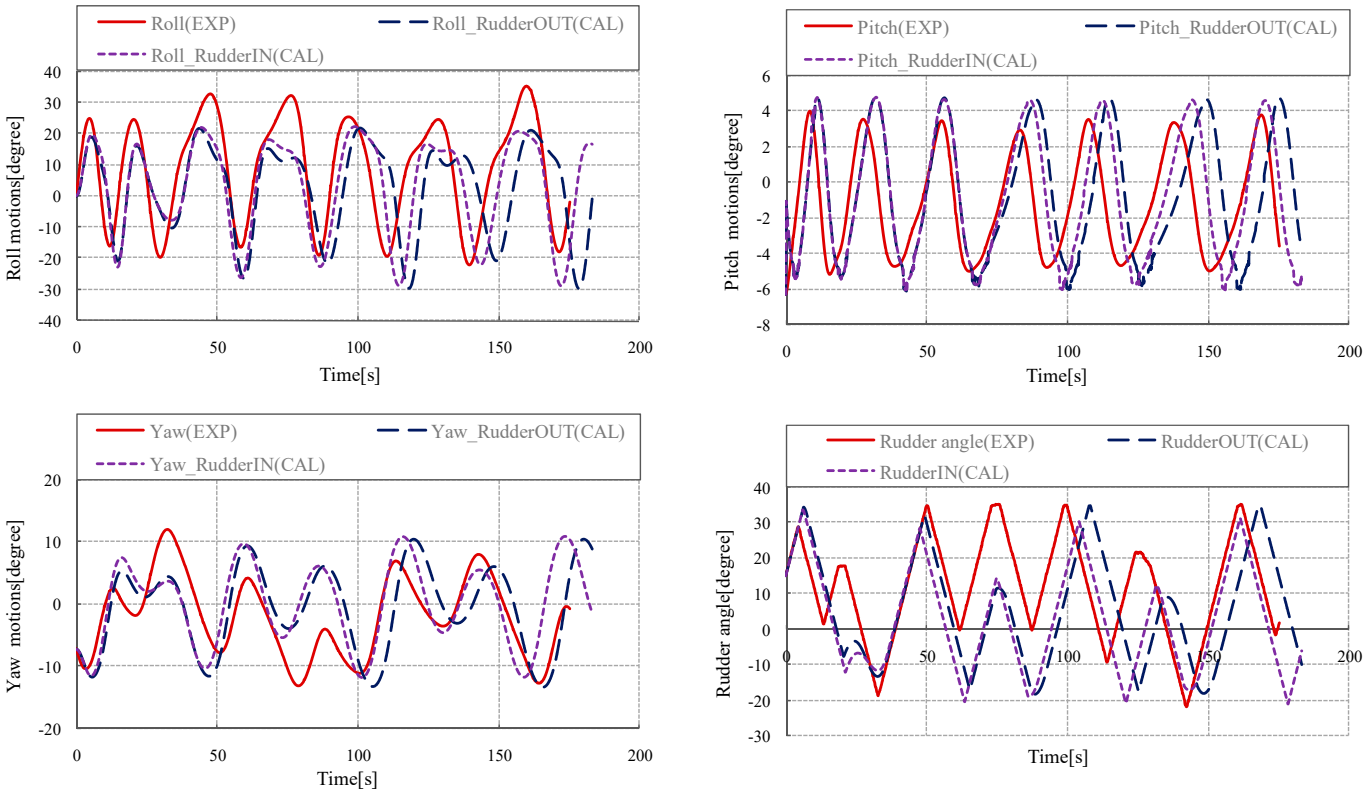

Figure 14. Comparison of time histories of ship motion with Fn = 0.35 (RudderIN (CAL): the calculation results without considering the rudder exposure in waves; RudderOUT (CAL): the calculation results considering the rudder exposure in waves; EXP: the experimental results).

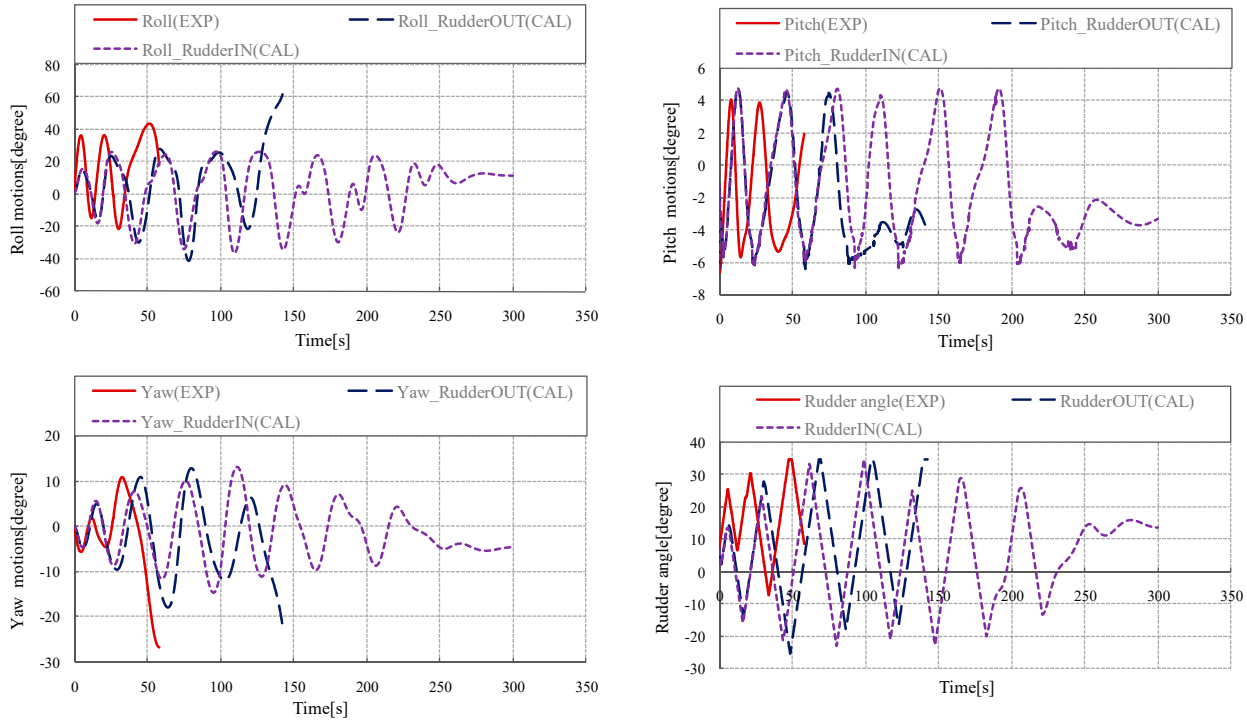

Figure 15. Comparison of time histories of ship motion with $Fn = 0.4$ (RudderIN (CAL): the calculation results without considering the rudder exposure in waves; RudderOUT (CAL): the calculation results considering the rudder exposure in waves; EXP: the experimental results).

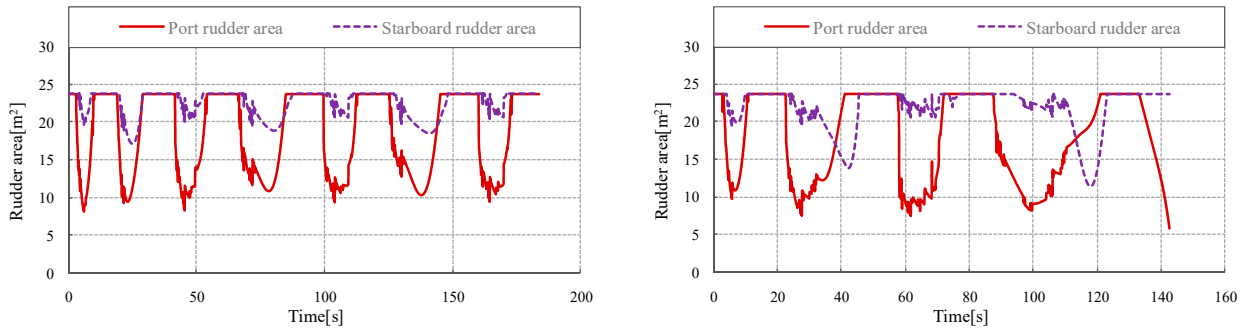

(**a**) $Fn = 0.35$ (**b**) $Fn = 0.4$

Figure 16. The time histories of rudder areas with $Fn = 0.35$ and $Fn = 0.4$ (RudderIN (CAL): the calculation results without considering the rudder exposure in waves; RudderOUT (CAL): the calculation results considering the rudder exposure in waves; EXP: the experimental results).

From Figures 14 and 16a, it can be seen that there is almost no difference in the ship's motion mode and motion amplitude between considering rudder exposure and not considering rudder exposure at the critical speed ($Fn = 0.35$). However, there is a small difference in the motion period. As the time goes on, the ship motions calculated by considering the rudder exposure lag slightly behind the calculation results without considering the rudder exposure and the experimental results.

From Figures 15 and 16b, considering the rudder exposure at a high speed ($Fn = 0.4$), a larger roll can cause the rudders to be out of the water, especially for the port rudder. Rudder exposure can reduce the rudder performance of the heading control, which can lead to a large deviation in the yaw direction. Even with the maximum rudder angle, it is impossible to control the heading, and broaching occurs. At the same time, the roll angle continues to increase, causing the ship to capsize.

However, the roll, pitch, yaw and rudder angle calculated without considering the rudder exposure gradually stabilize to constant values, and surf-riding eventually occurs. This indicates that the rudder exposure is a crucial factor for the prediction of broaching.

4.4. The Effect of Heave and Pitch Motions

The effect of heave and pitch motions on ship motion modes is analyzed. The comparison results of the time histories of ship motions with and without considering the heave and pitch motions are shown in Figures 17–19. The 6DOF calculations, which consider the heave and pitch motions, are written in Formulas (53) and (54). In addition, 4DOF represents the calculations without considering the heave and pitch motions, which are set to zero.

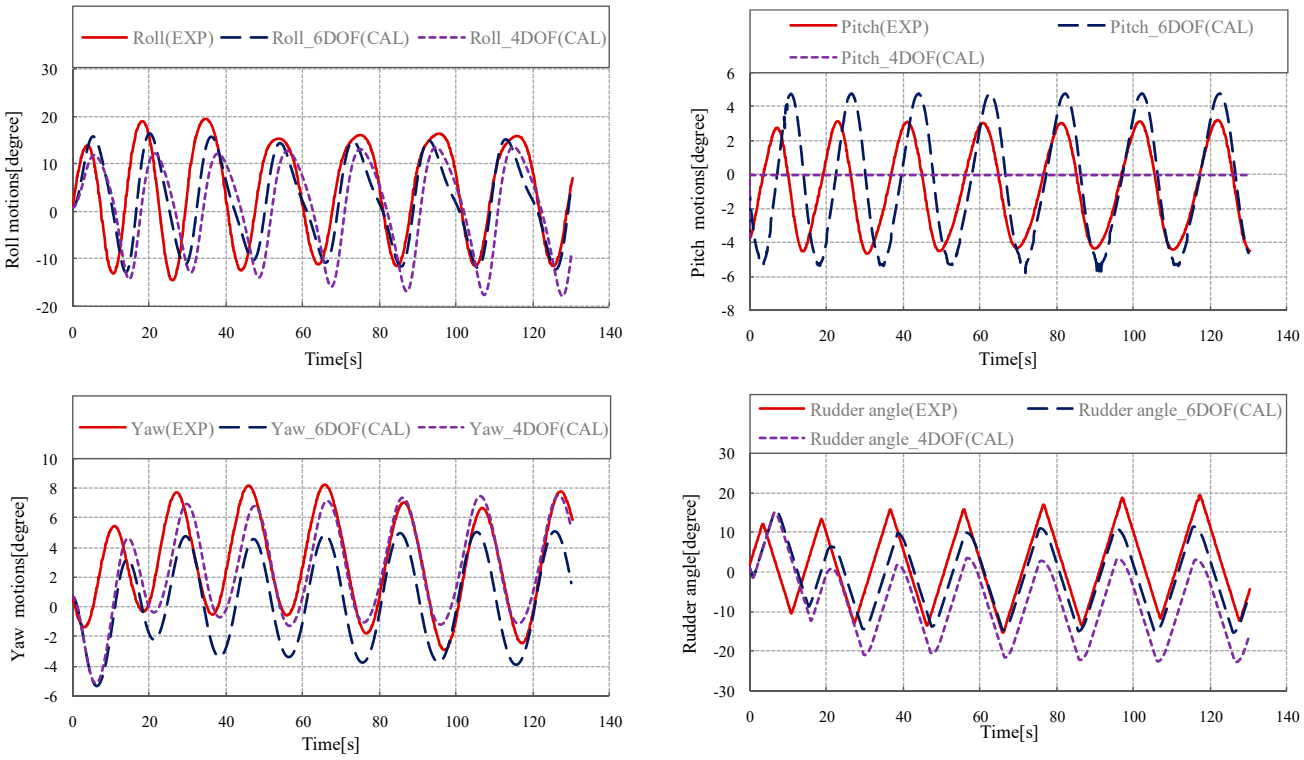

Figure 17. Comparison of time histories of ship motion with Fn = 0.25 (6DOF (CAL): the calculation results considering the heave and pitch motions; 4DOF (CAL): the calculation results without considering the heave and pitch motions; EXP: the experimental results).

Without considering heave and pitch, the calculated roll amplitude is larger because the roll motion is closely related to the heave and pitch motions. After considering the heave and pitch, the energy is transferred to heave and pitch motions, and the roll amplitude decreases.

The heave and pitch motions have a significant effect on the rudder-force model. When considering the rudder exposure, the combination of large roll, heave and pitch will increase the real-time area of the rudders being out of water, which results in broaching. However, without considering the heave and pitch, the ship ultimately only experiences stable surf-riding. This indicates that the heave and pitch motions have a significant effect on the prediction of broaching.

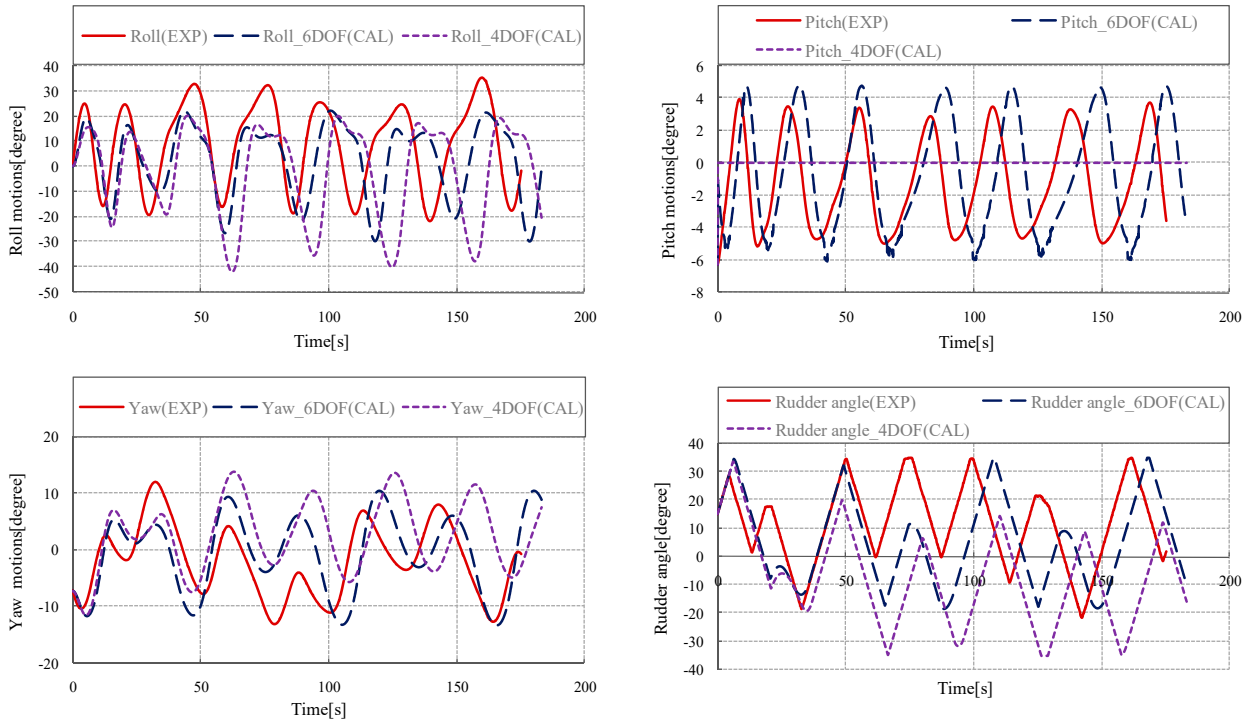

Figure 18. Comparison of time histories of ship motion with *Fn* = 0.35 (6DOF (CAL): the calculation results considering the heave and pitch motions; 4DOF (CAL): the calculation results without considering the heave and pitch motions; EXP: the experimental results).

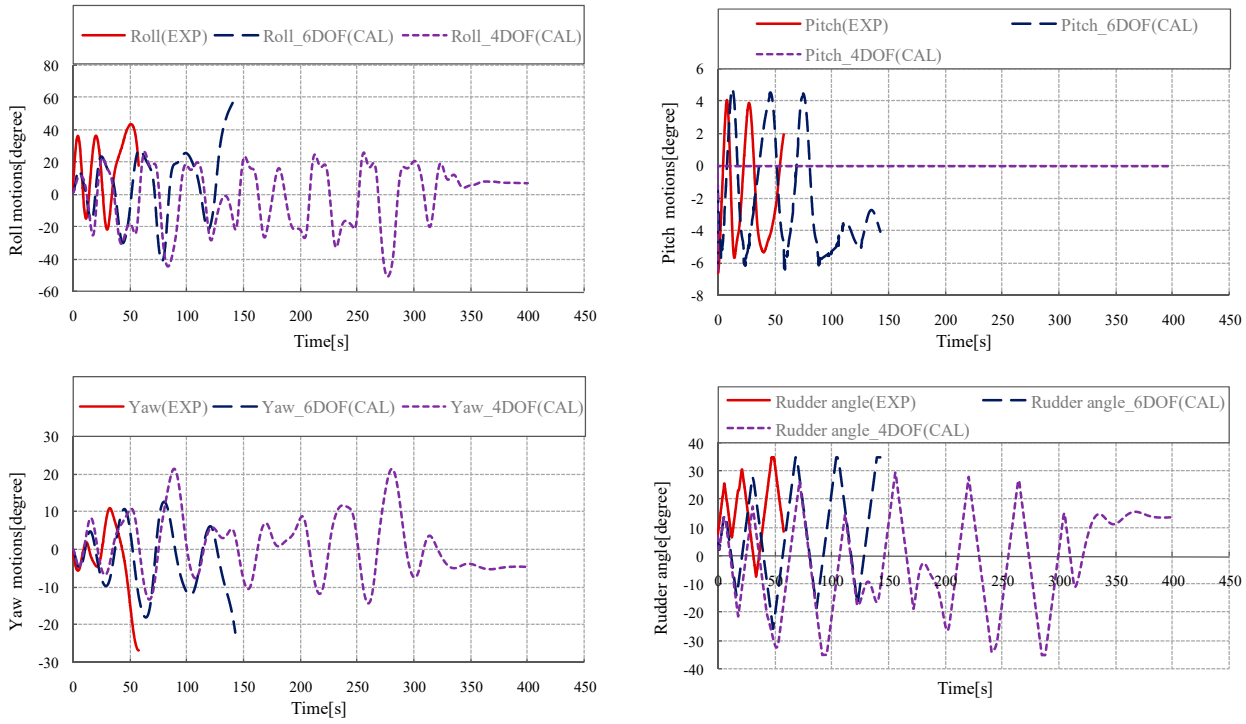

Figure 19. Comparison of time histories of ship motion with *Fn* = 0.4 (6DOF (CAL): the calculation results considering the heave and pitch motions; 4DOF (CAL): the calculation results without considering the heave and pitch motions; EXP: the experimental results).

5. Conclusions

To provide an accurate and efficient prediction method for the direct stability assessment of the surf-riding and broaching, an improved 6DOF mathematical model was established in this paper. Calculations and experiments with an ONR tumblehome vessel were performed in stern-quartering waves and the following remarks can be made:

(1) Through comparing the results of the calculations and experiments, it can be concluded that the recommended 6DOF coupled mathematical model can effectively predict broaching and pure loss of stability in stern-quartering waves. This prediction method can be used for the direct stability assessment of broaching and pure loss of stability. Combined with the criteria of the direct stability assessment, the prediction method can also be used to evaluate the stability of ships to guide ship design and evaluate the navigational performance of ships to guide ship maneuvering in waves.
(2) From the experiments and calculations, it can be seen that under the same wave condition and heading, as the speed increases, the motion mode of the ship transitions from pure loss of stability to broaching, which indicates that there is cross-coupling between the speed range of the occurrences of broaching and pure loss of stability. In addition, the significant roll caused by pure loss of stability can severely expose one side of the rudder in waves, which can result in a decrease in course-keeping capability. The significant roll induced by pure loss of stability is a key factor leading to broaching.
(3) The calculation considering the instantaneous wetted surface of the ship can effectively simulate the nonlinearity of roll motion, especially the large roll during broaching. The nonlinearity of roll has a significant effect on the prediction of broaching, which affects the final motion mode of the ship.
(4) The rudder exposure in waves is one of the key factors in predicting broaching.
(5) The heave and pitch affect the prediction accuracy of roll motion, and are also key factors affecting rudder exposure, which can reduce the course-keeping capability of rudders and result in broaching.

Author Contributions: Conceptualization, J.C. and M.G.; methodology, J.C.; software, J.C.; validation, J.C. and M.G.; formal analysis, J.C.; writing—original draft preparation, J.C.; writing—review and editing, P.Z. and J.L. All authors have read and agreed to the published version of the manuscript.

Funding: This research was funded by the National Natural Science Foundation of China (Grand No. 52271336).

Institutional Review Board Statement: Not applicable.

Informed Consent Statement: Not applicable.

Data Availability Statement: Data are contained within the article.

Conflicts of Interest: The authors declare no conflict of interest.

Nomenclature

List of symbols

a_{H}	Rudder force increase factor
AE, FE	After section and forward section of the hull
$F_{\mathrm{NP}}, F_{\mathrm{NS}}$	The port and starboard rudders normal forces
$f_{\alpha\mathrm{P}}, f_{\alpha\mathrm{S}}$	The port and starboard rudders lifting slope coefficients
g	Gravitational acceleration
I_{xx}, I_{zz}	Moment of inertia in roll and yaw
$J_{\mathrm{PP}}, J_{\mathrm{PS}}$	The port and starboard propellers advanced ratios
k	Wave number
K_{P}	Rudder gain coefficient

K_T	Thrust coefficient of the propeller
$\overline{\downarrow_R^{\gamma}}$	Mean correction factor for flow-straightening due to yaw
m	Ship mass
m_x	Ship-added mass in surge direction
m_y	Ship-added mass in sway direction
n_P	Propeller revolution
p	Roll rate
r	Yaw rate
S_F	Wetted hull surface area in still water
t_P	Thrust deduction factor
t_R	Steering resistance deduction factor
T_E	The time constant for the steering gear
T_D	The time constant for differential control
u, v	Surge and sway velocity of the ship hull
u_{RP}, u_{RS}	Inflow velocity to the port and starboard rudders in surge direction
v_R	Inflow velocity to the rudder in sway direction
w_P	Wake fraction at propeller position
x_{HR}, z_{HR}	Longitudinal and vertical positions of additional sway force due to the rud-der
x_R, z_R	Longitudinal and vertical positions of the rudder
α_{RP}, α_{RS}	Effective inflow angles to the port and starboard rudders
δ	Rudder angle
η	The ratio of propeller diameter to rudder span
ε	The ratio of wake fraction at the propeller and rudder position
κ	Propeller-induced flow velocity factor
λ	Wavelength
Λ	Ruder aspect ratio
Λ_P, Λ_S	The real-time port and starboard rudders aspect ratio
$\overline{\gamma_R}$	Mean flow-straightening effect coefficient
ρ	Water density
ω, ω_e	Wave frequency and encounter frequency
ζ_w	Wave amplitude

References

1. *MSC.1/Circ.1627*; Interim Guidelines on the Second-Generation Intact Stability Criteria. IMO: London, UK, 2020.
2. *SDC 8/WP.4*; Development of Explanatory Notes to the Interim Guidelines on Second Generation Intact Stability Criteria. IMO: London, UK, 2022.
3. Umeda, N.; Hashimoto, H. Qualitative Aspects of Nonlinear Ship Motions in Following and Quartering Seas with High Forward Velocity. *J. Mar. Sci. Technol.* **2002**, *6*, 111–121. [CrossRef]
4. Umeda, N.; Hashimoto, H. Broaching Prediction in the Light of an Enhanced Mathematical Model, with Higher-order Terms Taken into Account. *J. Mar. Sci. Technol.* **2003**, *7*, 145–155.
5. Hashimoto, H.; Umeda, N.; Matsuda, A. Importance of Several Nonlinear Factors on Broaching Prediction. *J. Mar. Sci. Technol.* **2004**, *9*, 80–93. [CrossRef]
6. Hashimoto, H.; Umeda, N.; Matsuda, A. Model Experiment on Heel-induced Hydrodynamic Forces in Waves for Realizing Quantitative Prediction of Broaching. *Fluid Mech. Its Appl.* **2011**, *96*, 379–398.
7. Hashimoto, H.; Umeda, N.; Matsuda, A. Broaching Prediction of a Wave-Piercing Tumblehome Vessel with Twin Screws and Twin Rudders. *J. Mar. Sci. Technol.* **2011**, *16*, 448–461. [CrossRef]
8. Araki, M.; Umeda, N.; Hashimoto, H.; Matsuda, A. Broaching Prediction Using an Improved System-Based Approach. In Proceedings of the 28th Symposium on Naval Hydrodynamics, Pasadena, CA, USA, 12–17 September 2010; pp. 1–12.
9. Araki, M.; Umeda, N.; Hashimoto, H.; Matsuda, A. An Improvement of Broaching Prediction with a Nonlinear 6 Degrees of Freedom Model. *J. Jpn. Soc. Nav. Archit. Ocean Eng.* **2011**, *14*, 85–96. [CrossRef]
10. Umeda, N.; Usada, S.; Mizumoto, K.; Matsuda, A. Broaching Probability for a Ship in Irregular Stern-quartering Waves: Theoretical Prediction and Experimental Validation. *J. Mar. Sci. Technol.* **2016**, *21*, 23–37. [CrossRef]
11. Htet, T.Z.; Umeda, N.; Maki, A.; Matsuda, A.; Terada, D. Estimation of Broaching Probability Using Wave-induced Forces and Moments Measured in Captive Model Tests. *J. Mar. Sci. Technol.* **2019**, *24*, 317–327. [CrossRef]

12. Spyrou, K.J.; Belenky, V.L.; Themelis, N.; Weems, K.M. Definitions of Celerity for Investigating Surf-riding in An Irregular Seaway. In *Fluid Mechanics and Its Applications, Contemporary Ideas on Ship Stability-Risk of Capsizing*; Springer: Cham, Switzerland, 2019; Volume 119, pp. 359–377.
13. Spyrou, K.J.; Themelis, N.; Kontolefas, I. Estimates of the Probability of Surf-Riding in Irregular Seas. In *Fluid Mechanics and Its Applications, Contemporary Ideas on Ship Stability—From Dynamics to Criteria*; Springer International Publishing: Cham, Switzerland, 2023; Volume 134, pp. 387–399.
14. Belenky, V.; Spyrou, K.; Weems, K. Critical Distance on a Phase Plane as a Metric for the Likelihood of Surf-Riding in Irregular Waves. In *Fluid Mechanics and Its Applications, Contemporary Ideas on Ship Stability—From Dynamics to Criteria*; Springer International Publishing: Cham, Switzerland, 2023; Volume 134, pp. 413–434.
15. Themelis, N.; Angelou, M.; Spyrou, K.J. Statistical Correlations of Ship High-run with Broaching-to and Capsize. *J. Mar. Sci. Eng.* **2020**, *8*, 846. [CrossRef]
16. Yu, L.W.; Qu, D.C.; Wang, S.Q.; Ma, N. On the Probability Estimates of Broaching in Irregular Waves by Direct Counting on Intensive Repeated Simulations. *Ocean Eng.* **2022**, *266*, 112854. [CrossRef]
17. Chu, J.L.; Lu, J.; Gu, M. Prediction Method for Surf-riding of Unconventional Tumblehome Ship. *J. Ship Mech.* **2022**, *26*, 1150–1159.
18. Khanfir, S.; Hasegawa, K.; Nagarajan, V.; Shouji, K.; Lee, S.K. Maneuvering Characteristics of Twin-rudder systems: Rudder-hull Interaction Effect on the Maneuverability of Twin-rudder Ships. *J. Mar. Sci. Technol.* **2011**, *16*, 472–490. [CrossRef]
19. *SDC 2/INF.10, Annex 35*; Working Version of Draft Explanatory Notes on the Vulnerability of Ships to the Broaching Stability Failure Model. IMO: London, UK, 2015.
20. Lu, J.; Umeda, N.; Ma, K. Predicting parametric rolling in irregular head seas with added resistance taken into account. *J. Mar. Sci. Technol.* **2011**, *16*, 462–471. [CrossRef]